Long non-coding RNA mitophagy and ALK-negative anaplastic lymphoma-associated transcript: a novel regulator of mitophagy in T-cell lymphoma

Valentina Mularoni,[1] Benedetta Donati,[1] Annalisa Tameni,[1] Veronica Manicardi,[1] Francesca Reggiani,[1] Elisabetta Sauta,[2] Magda Zanelli,[3] Marco Tigano,[4] Emanuele Vitale,[1,5] Federica Torricelli,[1] Stefano Ascani,[6] Giovanni Martino,[6,7] Giorgio Inghirami,[8] Francesca Sanguedolce,[9] Alessia Ruffini,[10] Alberto Bavieri,[10] Stefano Luminari,[10] Marco Pizzi,[11] Angelo Paolo Dei Tos,[11] Cinzia Fesce,[12] Antonino Neri,[13] Alessia Ciarrocchi[1] and Valentina Fragliasso[1]

[1]Laboratory of Translational Research, Azienda USL-IRCCS di Reggio Emilia, Reggio Emilia, Italy; [2]IRCCS Humanitas Clinical and Research Center, Milan, Italy; [3]Pathology Unit, Department of Oncology, Oncology, Azienda USL-IRCCS di Reggio Emilia, Reggio Emilia, Italy; [4]Sidney Kimmel Medical College, Thomas Jefferson University, Philadelphia, PA, USA; [5]Clinical and Experimental Medicine Ph.D. Program, University of Modena and Reggio Emilia, Modena, Italy; [6]Pathology Unit, Azienda Ospedaliera Santa Maria di Terni, University of Perugia, Terni, Italy; [7]Institute of Hematology and CREO, University of Perugia, Perugia, Italy; [8]Department of Pathology and Laboratory Medicine, Weill Cornell Medicine, New York, NY, USA; [9]Pathology Unit, Policlinico Riuniti, University of Foggia, Foggia, Italy; [10]Hematology Unit, Azienda USL-IRCCS di Reggio Emilia, Reggio Emilia, Italy; [11]Surgical Pathology & Cytopathology Unit, Department of Medicine-DIMED, University of Padova, Padova, Italy; [12]Hematology Unit, University Hospital, Foggia, Italy and [13]Scientific Directorate, Azienda USL-IRCCS di Reggio Emilia, Reggio Emilia, Italy

Correspondence: V. Fragliasso
Valentina.Fragliasso@ausl.re.it

Received: December 14, 2022.
Accepted: June 20, 2023.
Early view: June 29, 2023.

https://doi.org/10.3324/haematol.2022.282552

Abstract

Long non-coding RNA (lncRNA) are emerging as powerful and versatile regulators of transcriptional programs and distinctive biomarkers of progression of T-cell lymphoma. Their role in the aggressive anaplastic lymphoma kinase-negative (ALK$^-$) subtype of anaplastic large cell lymphoma (ALCL) has been elucidated only in part. Starting from our previously identified ALCL-associated lncRNA signature and performing digital gene expression profiling of a retrospective cohort of ALCL, we defined an 11 lncRNA signature able to discriminate among ALCL subtypes. We selected a not previously characterized lncRNA, MTAAT, with preferential expression in ALK$^-$ ALCL, for molecular and functional studies. We demonstrated that lncRNA MTAAT contributes to an aberrant mitochondrial turnover restraining mitophagy and promoting cellular proliferation. Functionally, lncRNA MTAAT acts as a repressor of a set of genes related to mitochondrial quality control via chromatin reorganization. Collectively, our work demonstrates the transcriptional role of lncRNA MTAAT in orchestrating a complex transcriptional program sustaining the progression of ALK$^-$ ALCL.

Introduction

T-cell lymphoma (TCL) is a complex and heterogeneous group of neoplasms with different biology and outcome.[1] Its diagnostic classification is still a challenge, making its treatment suboptimal. Anaplastic lymphoma kinase-negative (ALK$^-$) anaplastic large cell lymphoma (ALCL) is one of the most aggressive subtypes of TCL and is characterized by a dismal prognosis and high mortality.[2-4] The molecular details of the pathogenesis of ALK$^-$ ALCL are largely unknown, thus limiting the development of targeted strategies.[5] Therefore, clarifying the mechanisms underlying this disease is of utmost importance.

The fast and massive implementation of deep sequencing technologies has highlighted the role of the non-coding genome in regulating cancer proliferation, especially in complex tumors without a clear genetic driver.[6,7] Particular attention has been paid to a family of transcripts of about 200 bp with no coding potential, known as long non-coding RNA (lncRNA).[8] LncRNA possess the striking ability to interact with protein-coding and non-coding transcripts regulating and integrating a complex network of processes simultaneously.[9-12] Thanks to their peculiar and versatile features, lncRNA are able to influence – in a context-dependent manner – several aspects of cancer biology, such as cellular proliferation, apoptosis, metabolic reprogram-

ming, genomic instability, drug resistance, invasion, and metastasis.[13,14] Thus, deregulating the expression of certain lncRNA can directly influence the pathogenesis and/or progression of different types of cancers, including TCL.[15]
Previously, we investigated the contribution of lncRNA to ALCL pathogenesis by performing deep transcriptomic profiling of a cohort of ALCL. We identified a unique set of 18 lncRNA overexpressed in neoplastic T-lymphocytes compared to normal T-lymphocytes.[16] We were able to show that among those, the lncRNA *BlackMamba* acts as a major transcriptional regulator of neoplastic T-lymphocytes in the ALK$^-$ ALCL subtype, influencing lymphoma progression.[16,17] Therefore, the identified lncRNA are not only distinctive biomarkers of disease but also play relevant functional roles in the biogenesis of ALCL.
In this work, we expand our knowledge regarding the functional relevance of lncRNA in the development and progression of ALCL. Starting from our previously identified lncRNA signature and integrating the gene expression profiles of a large cohort of ALCL patients with clinical information, we defined a powerful lncRNA signature that discriminates between ALK$^-$ and ALK$^+$ subtypes. We then focused on the XLOC_211989 transcript – which resulted specifically associated with the ALK$^-$ ALCL subtype – and characterized its function by using multiple functional approaches. Our data suggest that this non-coding transcript coordinates the expression of a set of genes involved in mitochondrial homeostasis and mitophagy promoting lymphoma cell survival. We named this novel lncRNA *MiTophagy and ALK$^-$ Anaplastic Lymphoma Associated Transcript* (MTAAT).

Methods

Patients' specimens

Fresh and viable cryopreserved cells and formalin-fixed paraffin-embedded (FFPE) sections of two retrospective cohorts of ALCL were isolated from diagnostic/relapsed primary lymphoma biopsies. Diagnoses were assigned according to the World Health Organization classification.[1] Tissues used for expression analyses were selected for their high tumor cell content (>50%). The FFPE cohort of samples of ALCL consisted of 54 cases whereas the freshly frozen cohort of samples consisted of 18 ALCL cases. Regarding clinicopathological characteristics of the FFPE cohort eligible for the analysis (n=44), among ALK$^-$ ALCL, 17/29 (59%) patients were male and the median age was 70 years (range, 31-88). Regarding ALK$^+$ ALCL, 8/15 (53%) patients were male and the median age was 39 years (range, 21-75). Considering follow-up data available for 29/44 patients, the median follow-up of the cohort was 44 months (range, 2.2-152). The 4-year progression-free survival rate was 70.6% (95% confidence interval: 55.2-90.3). The freshly frozen cohort of ALCL and immunophenotypic features of resting and donor CD4$^+$ T-lymphocytes have been described previously.[16]
The study was approved through institutional human ethics review boards of the Ethical Committee AVEN and AUSL-IRCCS of Reggio Emilia (287/2018/OSS/IRCCSRE), and patients provided written informed consent in accordance with the Declaration of Helsinki.

RNA extraction and quantitative polymerase chain reaction

Total RNA from cells was extracted by TRIzol (Thermo Fisher Scientific) according to the manufacturer's instructions. One microgram of total RNA was retrotranscribed using the iScript cDNA kit, (Biorad). The amplified transcript level of each specific gene was normalized on the *CHMP2A* housekeeping gene. The ΔΔCt quantification method was used for quantitative polymerase chain reaction (RT-qPCR) analyses. The list of primers used is provided in *Online Supplementary Table S1*.

Antisense LNA GapmeR transfection

MAC2A and TLBR-2 cells (1×10^6) were transfected with 50 nM Antisense LNA GapmeR for a single knockdown (KD). Antisense LNA GapmeR transfections were performed using the Cell Line Nucleofector Kit SF and Amaxa 4D Nucleofector (program DS-130 for TLBR-2; FI115 for MAC2A). Twenty-four hours after transfection, cells were harvested and plated at 2.5×10^5 cells/mL. Antisense LNA GapmeR Negative Control (Cat. N/ID: 33951, Qiagen) was used as a negative control. For lncRNA_211989/MTAAT we used two different GapmeRs (Cat. N/ID: 339511, Qiagen); their sequences are provided in *Online Supplementary Table S2*.

Mitochondrial staining

Mitochondria were stained with Mitotracker (Thermo Fisher Scientific) according to the manufacturer's instructions. Cells were then harvested, fixed in 4% paraformaldehyde in phosphate-buffered saline (PBS) 1X for 10 min at room temperature, and spotted on glass slides using Cytospin (Thermo Scientific) as previously reported.[18] Dots were washed in PBS 1X three times and nuclei were stained with DAPI.
Tetramethylrhodamine methyl ester perchlorate (TMRM) staining was performed according to the manufacturer's instructions (Thermo Fisher Scientific), without substantial changes. Cells were then harvested and washed once in RPMI medium without serum. Membrane potential was immediately measured by flow cytometry with a FACSCanto™ II Cell Analyzer (BD Biosciences).

Statistical analysis

Statistical analyses were performed using GraphPad Prism software (GraphPad). Statistical significance was deter-

mined using a Student *t* test. Each experiment was replicated multiple times (>3 up to 6). All analyses were performed using R software version 4.1.3.

Results

XLOC_211989 is a novel biomarker that stratifies patients with ALK⁻ anaplastic large cell lymphoma

We assessed whether the previously generated ALCL-associated lncRNA signature[16] might be used to distinguish ALCL subtypes in a retrospective cohort of 54 ALCL cases. Gene expression analyses were performed by digital multiplexing profiling using a custom panel of probes targeting the 17 previously identified lncRNA and four additional genes used for the molecular classification of ALCL subtypes.[19]

Out of the total of 54 samples, 44 ALCL gene expression profiles passed stringent quality controls and resulted eligible for the analysis (Figure 1A). Of these 44 samples, 15 (34%) were classified as ALK⁺ ALCL and 29 (66%) scored as ALK⁻ ALCL (Figure 1A, *Online Supplementary Figure S1A, B, Online Supplementary Table S4*). Focusing on lncRNA, we confirmed that 17/17 (100%) lncRNA were expressed in the ALCL cohort. Principal component analysis showed that lncRNA expression profiles segregated well with ALK⁺ and ALK⁻ ALCL samples (Figure 1B) resulting in 11 of the 17 (65%) lncRNA significantly deregulated between the two subtypes (Figure 1C, *Online Supplementary Figure S1C*). In particular: seven lncRNA were overexpressed in ALK⁻ ALCL

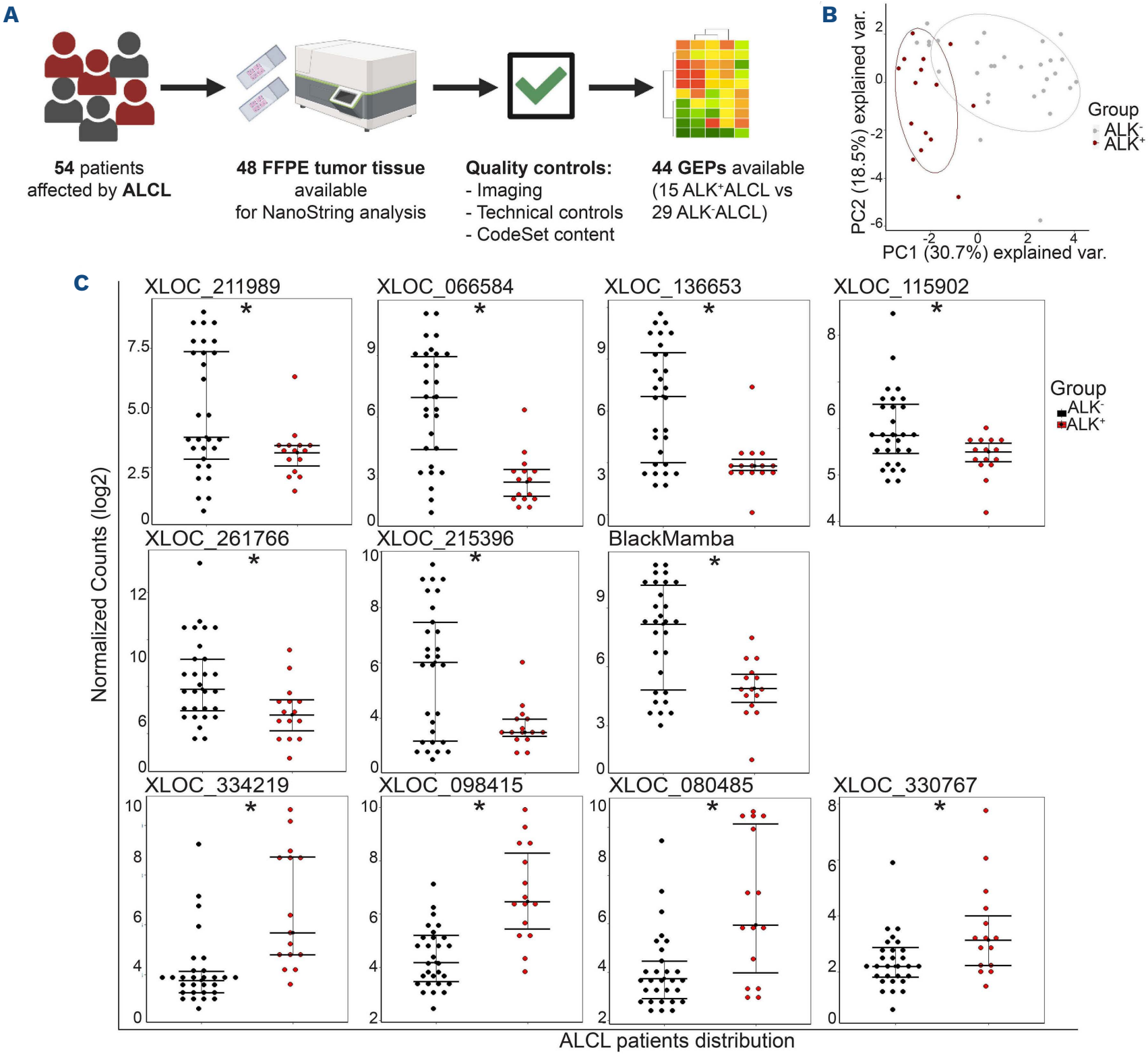

Continued on following page.

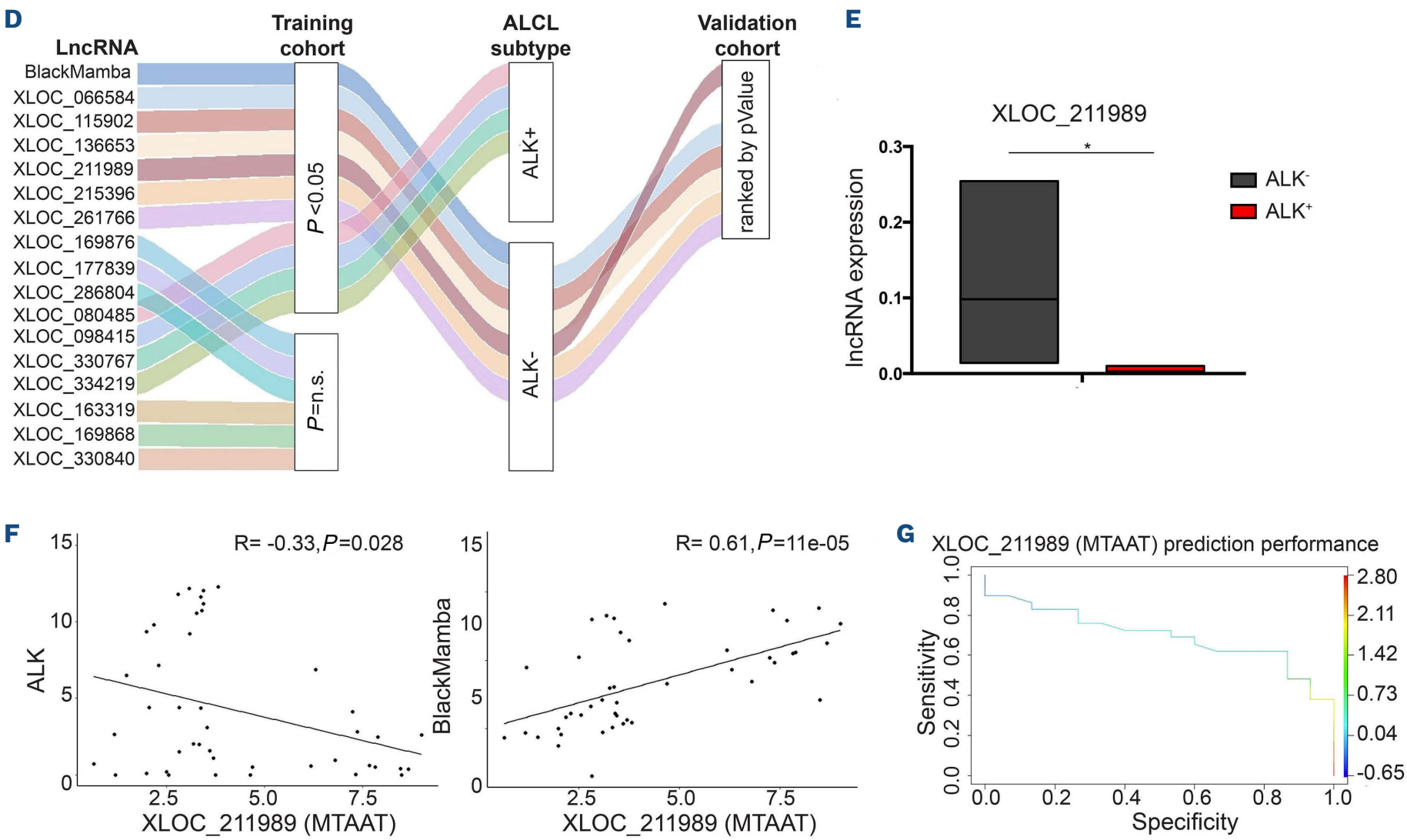

Figure 1. XLOC_211989 stratifies patients with ALK– anaplastic large cell lymphoma. (A) Outline of the study workflow for the formalin-fixed paraffin-embedded (FFPE) training cohort of samples to classify patients with anaplastic large cell lymphoma (ALCL) based on transcriptomic profiles. Figure created with BioRender.com. (B) Principal component analysis shows the variance between ALK⁺ ALCL (red dots) and ALK⁻ ALCL (gray dots) samples of the FFPE training cohort explained by the expression level of the 17 long non-coding RNA (lncRNA). (C) Dot plots show the distributions of gene expression counts of the 11 statistically significant lncRNA among ALK⁺ ALCL (red dots) and ALK⁻ ALCL (black dots) of the FFPE training cohort. Comparisons were considered statistically significant for $P \leq 0.05$ (*). (D) An alluvial plot shows the workflow for the identification and validation of XLOC_211989. (E) Box plot representing the expression of XLOC_211989 among ALK⁺ (red) and ALK⁻ (gray) ALCL evaluated by quantitative polymerase chain reaction in the validation cohort. The comparison was considered statistically significant for $P \leq 0.05$ (*). (F) Correlation plot between ALK and XLOC_211989 normalized and $\log_2$ transformed gene counts in the FFPE training cohort (left panel). Correlation plot between BlackMamba and XLOC_211989 normalized and $\log_2$-transformed gene counts in the training cohort (right panel). (G) Receiver operating characteristic curve showing the performance of the XLOC_211989-based scoring system in the training cohort of ALCL patients. The curve is colored according to XLOC_211989 adjusted values, the relation between colors and different values is represented by the bar on the right. The formula was generated by a generalized linear regression model.

patients while four lncRNA were overexpressed in ALK⁺ ALCL patients (Figure 1C). In accordance with our previous observations,[16] lncRNA *BlackMamba* showed a significant, negative correlation with ALK expression (Figure 1C).

We focused our attention on the six uncharacterized lncRNA that were significantly associated with the ALK⁻ subtype (Figure 1D). First, we confirmed their association with the ALK⁻ subtype by targeted RT-qPCR performed in a previously published cohort of 15 freshly frozen ALCL.[16] From this analysis, XLOC_211989 – herein named lncRNA MTAAT – showed the strongest and most significant association with ALK⁻ ALCL (Figure 1D, E, *Online Supplementary Figure S1D*). No detectable MTAAT expression was observed in donor resting or activated CD4⁺ cells (*Online Supplementary Figure S1E*), further confirming ALCL-restricted MTAAT expression.

To strengthen these observations, we explored the correlation between MTAAT and ALK expression in the retrospective cohort of ALCL samples. Linear regression analysis showed that MTAAT was inversely correlated with ALK expression and positively correlated with lncRNA *BlackMamba* (Figure 1F). The receiver operating characteristic curve for ALK subtype classification showed that MTAAT has a high capacity (70%) to discriminate between ALK⁻ and ALK⁺ patients (area under the curve=0.70; 95% confidence interval: 0.54-0.85) (Figure 1G, *Online Supplementary Figure S1F*).

The MTAAT promoter is bound by RNA polymerase II and enriched for active histone marks

Genomic annotation showed that the MTAAT sequence matches an uncharacterized intergenic transcript en-

coded on the plus strand of chromosome 3 with an estimated transcript length of 7,189 bp and no predicted alternative isoforms (Figure 2A). *In silico* analysis predicted four potential open reading frames with irrelevant coding potential within the MTAAT sequence, confirming the non-coding nature of this transcript (*Online Supplementary Table S5*).

Given the specificity of MTAAT expression in the ALK$^-$ ALCL subtype, we sought to define *in vitro* the molecular mechanisms that control its expression. For this analysis, we chose the two ALK$^-$ ALCL cell lines, TLBR-2 and MAC2A, displaying the highest levels of MTAAT expression (*Online Supplementary Figure S2A*). To identify the promoter of MTAAT, we first analyzed RNA polymerase II (RNAPII) genomic occupancy and histone 3 trimethyl lysine 4 (H3K4me3) profile using chromatin immunoprecipitation (ChIP) followed by sequencing in TLBR-2 cells. A high-density distribution of RNAPII within a 2000 bp region spanning the putative transcription start site (TSS) of MTAAT (P3-P6) was observed. This region was also enriched in H3K4me3, confirming the promoter-like nature of its sequence (Figure 2A). We confirmed the findings by ChIP-qPCR in both TLBR-2 and MAC2A cell lines (Figure 2B, C, *Online Supplementary Figure S2B*). We also showed that this region is marked by a high level of histone H3 acetyl-lysine 27 (H3K27ac) confirming that this locus is transcriptionally active in these cellular models (Figure 2D, *Online Supplementary Figure S2B*). Notably, ChIP-qPCR analysis did not show RNAPII or histone modification enrichment in a cell line, CUTLL1, negative for MTAAT expression (*Online Supplementary Figure S2C*), validating the specificity of our observations. To assess whether the putative promoter of MTAAT is able to transactivate transcription, we cloned the 2000 bp DNA sequence spanning from –1,500 bp to +500 bp of the MTAAT-TSS upstream of a luciferase reporter cassette. In this “promoter-like” configuration, high luciferase activity was detected in both MAC2A and TLBR-2 cells (Figure 2E).

Next, we searched for the signaling pathways underlying MTAAT expression. Based on the genomic profiles observed in ChIP-sequencing, we selected a 500 bp region spanning the TSS of MTAAT and performed a motif search analysis to identify potential transcription factor binding sites. For this, we used the FIMO analysis pipeline[20] and identified 117 hypothetical transcription factors (*Online Supplementary Table S6*). Notably, some transcription factors, including STAT, GATA, and IRF family members, are pertinent to signaling pathways known to be active and deregulated in ALK$^-$ ALCL[5] (Figure 2F). Specifically, we found a significant enrichment of several pathways related to the cellular response to cytokines, interferon, interleukins, and regulation of T-cell differentiation.

MTAAT is a chromatin-associated long non-coding RNA essential for the transcriptional control of mitochondrial processes

To examine the biological role of MTAAT in TCL, we first studied MTAAT cellular localization performing subcellular fractionation. We found that MTAAT was enriched in the nucleus and strongly associated with the chromatin fraction of lymphoma cells (Figure 3A, *Online Supplementary Figure S3A*) suggesting a putative role in chromatin organization and gene expression regulation. To investigate the role of this lncRNA in regulating lymphoma transcription, we silenced MTAAT expression by targeting different regions, single or in combination, with gapmer technology. MTAAT expression was measured by RT-qPCR and the delivery of multiple gapmers by electroporation resulted in effective knockdown (KD) (>50%) of MTAAT across all ALK$^-$ ALCL cell lines tested (Figure 3B). We then used next-generation RNA sequencing to evaluate the genome-wide transcriptional changes triggered by MTAAT silencing (MTAAT^{KD}). TLBR-2 cells were subjected to MTAAT^{KD} and RNA was collected 24 h after. In parallel and as a control, a scrambled gapmer was also delivered. RNA-sequencing analysis revealed 2,217 differentially expressed genes in MTAAT^{KD} compared to the gapmer control. Among these, 67.5% (1,497 genes) were protein-coding. Specifically, we detected 524 downregulated and 937 upregulated genes upon lncRNA MTAAT^{KD} (false discovery rate <0.1) (Figure 3C). These findings suggest a role for MTAAT in both the activation and the repression of transcription. Notably, the genomic regions of MTAAT targets are far beyond chromosome 3 (Figure 3D). This suggests that MTAAT could regulate ALK$^-$ ALCL transcriptional programs *in trans* and at a genome-wide level.

Gene-set enrichment analysis revealed diverse biological processes associated with deregulated genes. Specifically, downregulated transcripts showed significant enrichment in several gene sets related to mitochondrial respiratory chain complexes, DNA damage response, and chromatin organization. In contrast, upregulated transcripts are mostly implicated in immune response, glycolytic process, integrated stress response as well as regulation of mitochondrion organization (Figure 3E). Using RT-qPCR, we validated a representative set of upregulated genes confirming the RNA-sequencing results (Figure 3F).

To exclude off-target effects of the gapmers designed for MTAAT^{KD}, we decided to corroborate the results by silencing MTAAT with a CRISPR-interference system, by using doxycycline-inducible dCas9-KRAB and two different single-guide RNA targeting the MTAAT promoter. Following lentiviral transduction of ALK$^-$ ALCL cells, we induced dCas9-KRAB for 48 h with doxycycline and evaluated MTAAT expression. RT-qPCR confirmed that both single-guide RNA repressed the level of MTAAT by >60% (*Online Supplementary Figure S3B-D*). Importantly, the expression

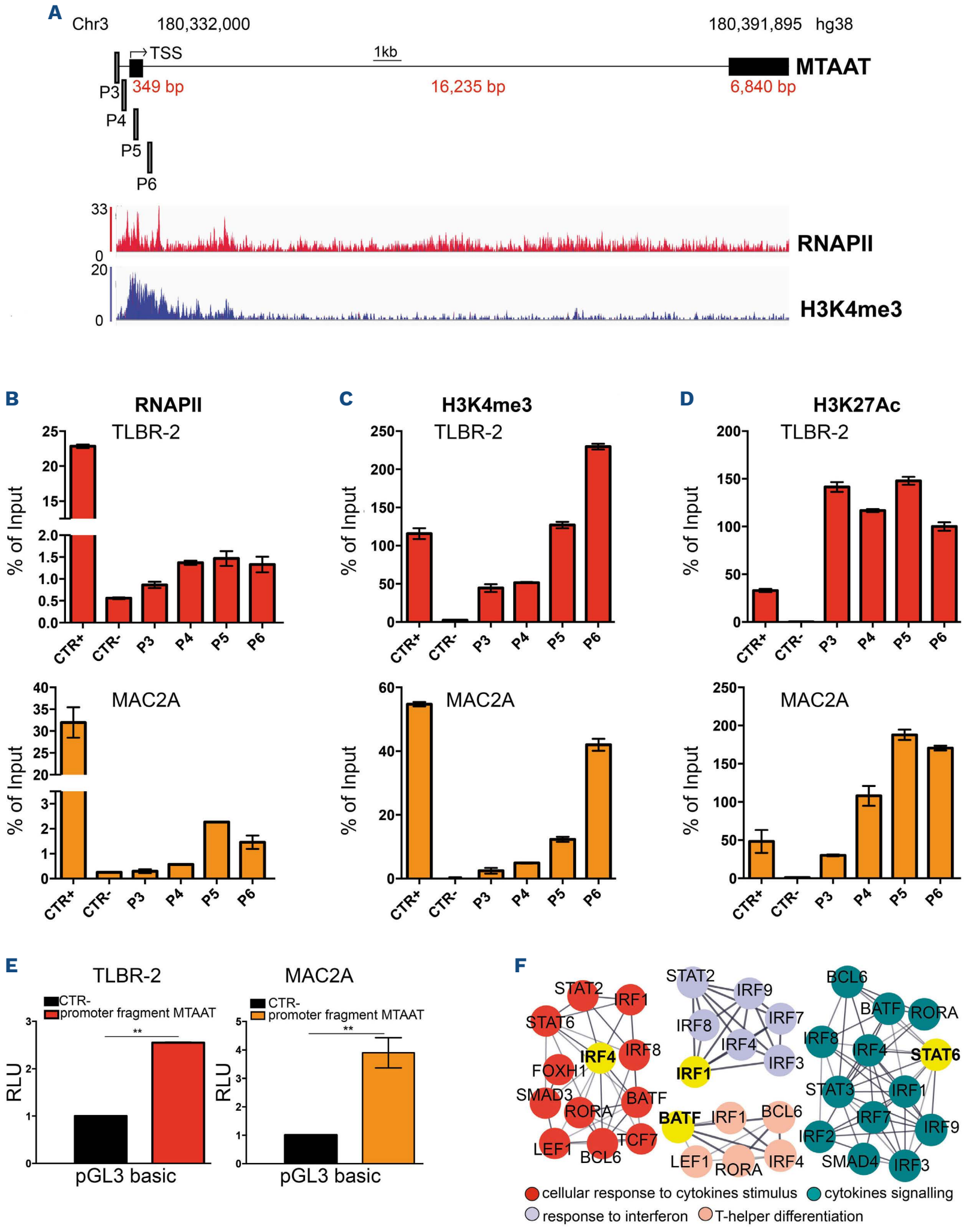

Figure 2. MTAAT is a novel long non-coding RNA. (A) Schematic representation of the locus and structure of MTAAT showing the position and enrichment level of active marks of transcription assessed by chromatin immunoprecipitation (ChIP) sequencing in TLBR-2 cells. (B-D) ChIP-quantitative polymerase chain reaction detection of RNAPII (B), H3K4me3 (C), and H3K27Ac (D) markers on MTAAT fragments in ALK$^-$ anaplastic large cell lymphoma (ALCL) cell lines. The GAPDH promoter was used as a positive control (CTR+) whereas a non-coding intergenic region served as a negative control (CTR–). The values are representative of three independent experiments. (E) Luciferase activity of the MTAAT fragment in a pGL3 vector. Data are represented as a normalized ratio of firefly-Renilla luciferase activities and are expressed as mean values ± standard deviation (N=3). $^{**}P \leq 0.01$. (F) Graphs show the most representative enriched transcription factor-related pathways. For each pathway, the transcription factor with the major number of interactions is colored in yellow. These graphs were created using cytoskape software.

of 10/12 (83%) gene targets after dCas9-KRAB-mediated MTAAT silencing was consistent with gapmer MTAAT^{KD}, ruling out any off-target effects (*Online Supplementary Figure S3E*). Collectively, the transcriptional changes that we observed upon MTAAT^{KD} indicated that this lncRNA acts as a repressor of a set of genes related to mitochondrial quality control.

MTAAT represses BNIP3 and BNIP3L via histone modifications

To understand how the lncRNA MTAAT regulates the expression of mitochondria-related genes, we evaluated changes in the chromatin organization triggered upon MTAAT^{KD} investigating, by ChIP, the distribution of H3K4Me3, H3K27Ac, and RNAPII on BCL2 Interacting Protein 3 (BNIP3) and BCL2 Interacting Protein 3 Like (BNIP3L also known as NIX). These proteins resulted in target genes of lncRNA MTAAT and their loss has been implicated in the accumulation of dysfunctional mitochondria in the hematopoietic system.[21,22] After the depletion of MTAAT, H3K4Me3 and H3K27Ac levels increased significantly in BNIP3 and BNIP3L promoters (Figure 4A-C). Likewise, RNAPII was found to be dramatically enriched around the TSS of both genes upon MTAAT^{KD} (Figure 4D). Similar changes were observed in additional MTAAT target genes such as Activating Transcriptional Factor 4 (ATF4) and X-Box Binding Protein 1 (XBP1) (*Online Supplementary Figure S4A-D*). Concordantly with the gene expression profile, no changes were observed in Optineurin (OPTN) gene *(Online Supplementary Figure S4A-E*). Furthermore, *in silico* analysis performed with catRAPID[23] showed a high interaction propensity of MTAAT with H3K27 methylation complex (*Online Supplementary Figure S4F*). Collectively, these data confirm that changes in chromatin markers are directly linked to the activity of MTAAT on its target genes.

To strengthen the clinical relevance of MTAAT regulation on these genes, we investigated the expression of BNIP3 and BNIP3L in the retrospective cohort of ALCL included in this study. In line with the repressive effect of MTAAT, BNIP3 expression was lower in ALK$^-$ ALCL than in ALK$^+$

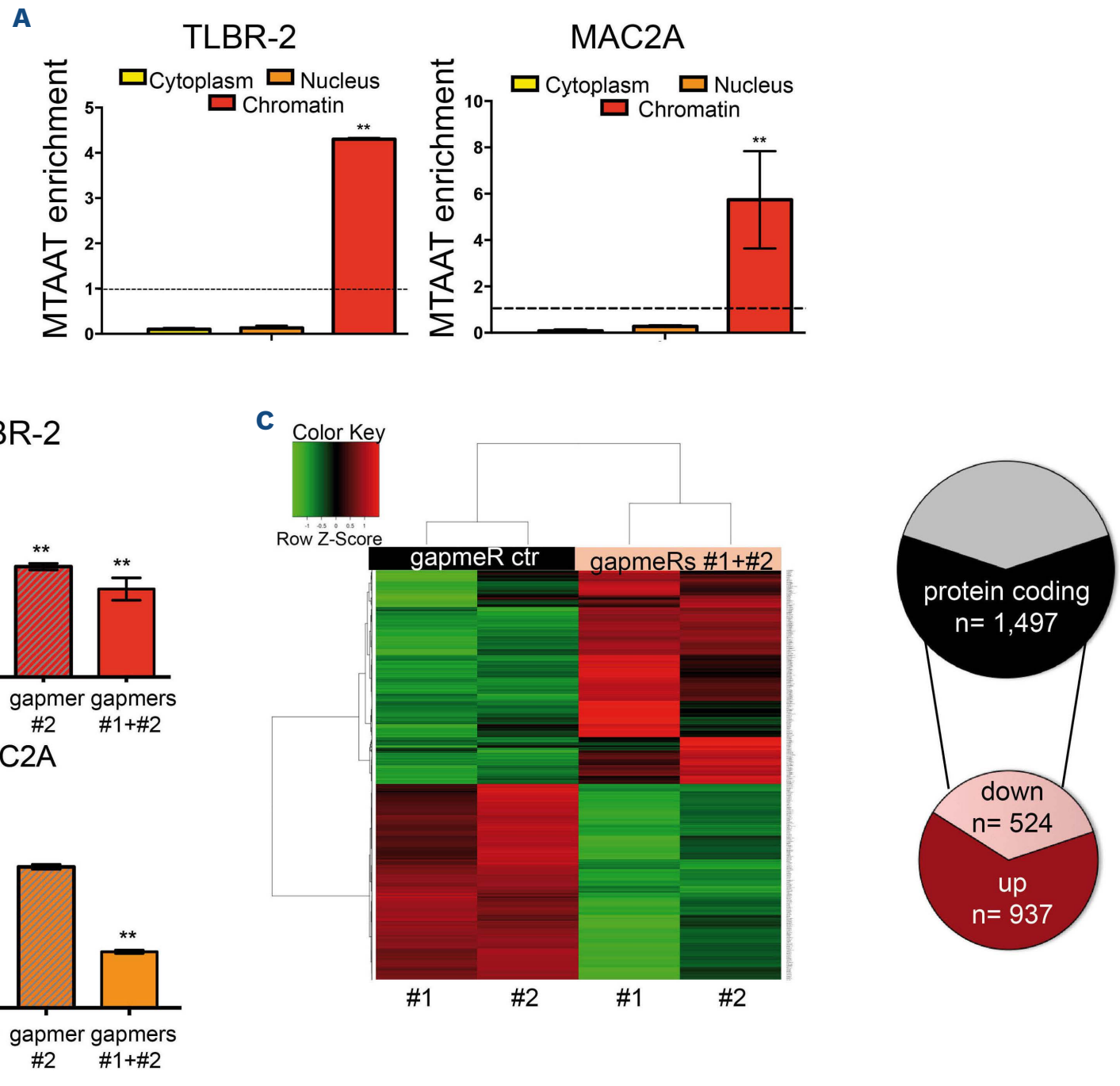

Continued on following page.

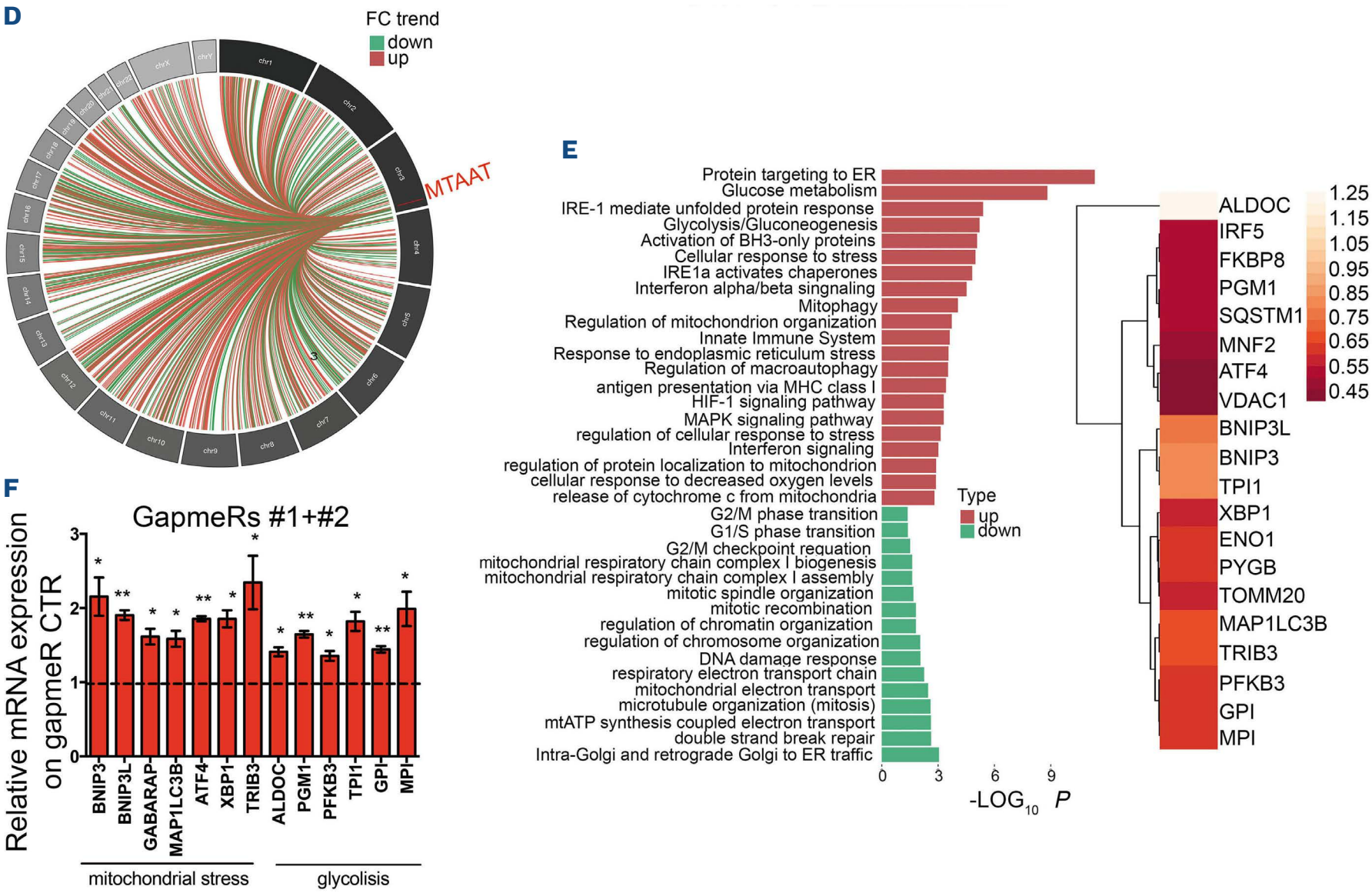

Figure 3. MTAAT knockdown results in transcriptional changes. (A) Relative expression of MTAAT in the cytoplasm, nucleus, and chromatin fraction of ALK$^-$ anaplastic large cell lymphoma (ALCL) cell lines (average of three independent experiments ± standard deviation). One-tailed *t* test, ***P*≤0.01. (B) Quantitative polymerase chain reaction (RT-qPCR) analysis of MTAAT expression 24 h after gapmer nucleofection in MAC2A and TLBR-2 cells. One-tailed *t* test, ***P*≤0.01. (C) The heatmap depicts hierarchical clustering based on 2,217 differentially expressed genes, whose read counts are Z-score normalized. Unsupervised hierarchical clustering was performed between gapmer control and gapmer #1+#2 samples (as indicated by the colored bar on columns) with a complete linkage method. Color intensity for each gene shows Z-score values ranging from red for upregulation to green for downregulation (left panel). The graph shows the number and the category of deregulated genes after RNA sequencing in TLBR-2 nucleofected with gapmers #1+#2 compared to gapmer control. (D) The circular plot displays the genomic location of MTAAT (highlighted with a red line) and the protein-coding genes differentially expressed upon its knockdown. Red links connect the long non-coding (lncRNA) MTAAT to upregulated genes, green links connect the lncRNA MTAAT to downregulated genes (right panel). (E) Most significantly enriched pathways (adjusted *P*<0.05) are represented showing the number of up- and down-regulated differentially expressed genes mapped in each considered pathway (left panel). The heatmap depicts validated significantly downregulated genes. The orange-red color bar shows the fold difference on the $\log_2$ scale calculated between doxycycline-treated and control samples. Lighter orange represents the most downregulated genes (right panel). (F) RT-qPCR validation of significantly upregulated genes obtained from RNA sequencing in TLBR-2 cells after nucleofection with gapmers (24 h). Each datum represents the mean ± standard error of mean (N=3). Two-tailed *t* test, **P*<0.05; ***P*<0.01.

ALCL patients (Figure 4E). A similar gene expression correlation was observed in a panel of non-TCL cell lines (*Online Supplementary Figure S4G*). In contrast, no significant differences were observed between ALCL subtypes for BNIP3L expression (Figure 4E).

MTAAT sustains the growth of anaplastic large cell lymphoma by regulating mitophagy

The transcriptional changes observed upon MTAAT^{KD} are suggestive of specific disruptions in mitochondrial homeostasis, such as an aberrant increase in mitochondrial density or changes in mitochondrial morphology. We wondered whether MTAAT promotes ALCL progression by controlling mitochondrial clearance. First, we investigated whether mitochondrial abundance changes in TCL upon dCas9-KRAB-inducible MTAAT^{KD}. We evaluated mitochondrial mass by Mitotracker staining and cytofluorimetric analysis. This analysis showed a time-dependent reduction in Mitotracker intensity signal upon MTAAT^{KD} (Figure 5A), whereas doxycycline treatment alone did not lead to changes (*data not shown*). Along the same line of evidence, we observed a strong reduction in mitochondrial DNA copy number, as determined by RT-qPCR analysis of the mitochondrial gene ND1 (Figure 5B). Furthermore, the steady-state level of sev-

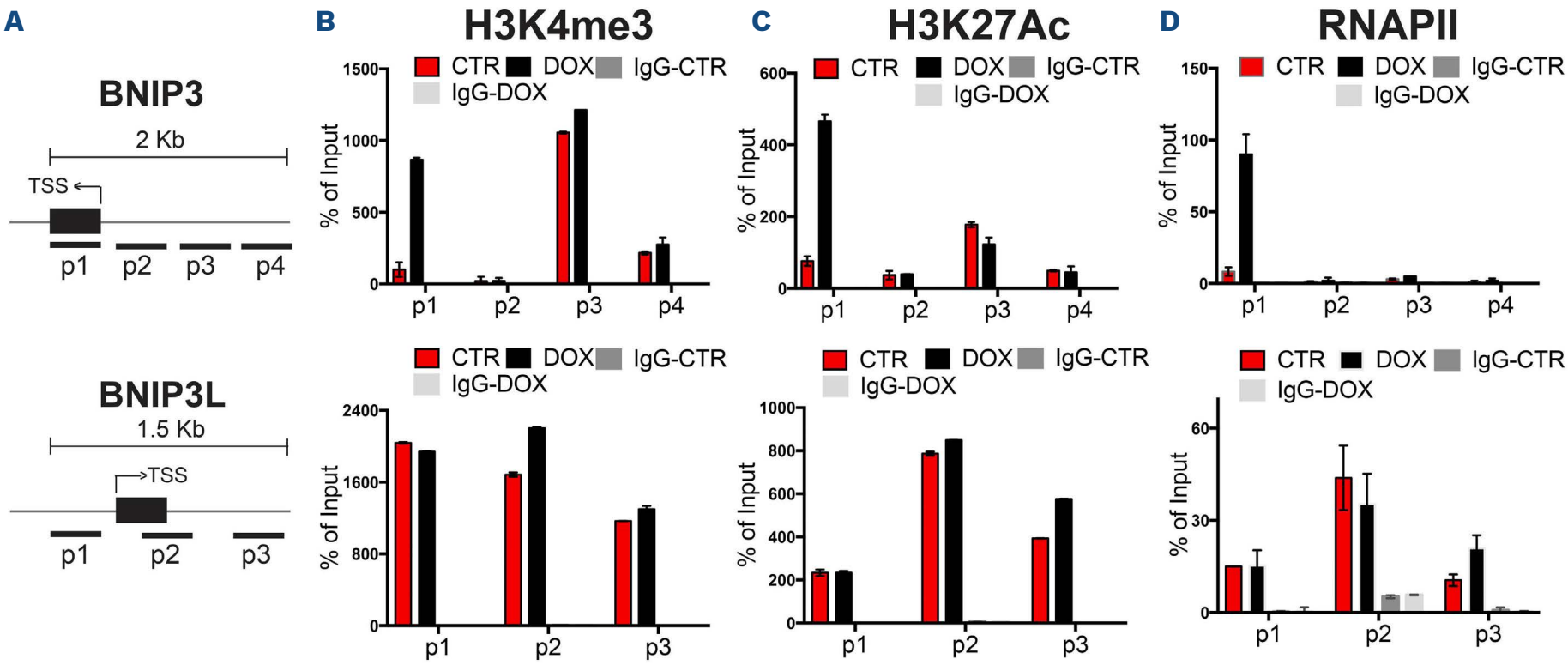

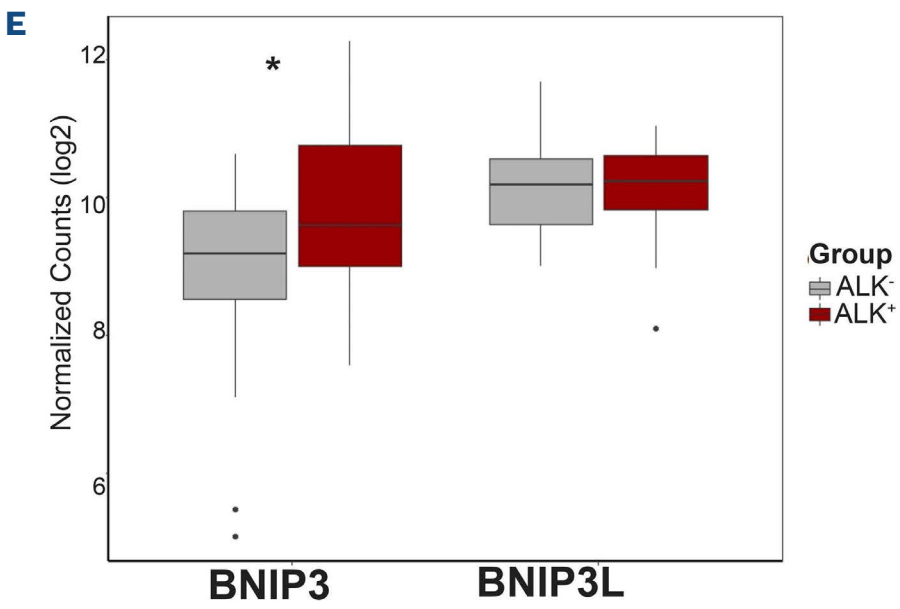

Figure 4. MTAAT knockdown modifies active transcriptional markers on regulatory elements of gene targets of MTAAT. (A) Graphs show the transcription start site (TSS) and fragments around the TSS of BNIP3 and BNIP3L. (B-D) Chromatin immunoprecipitation and quantitative polymerase chain reaction detection of H3K4me3 (B), H3K27Ac (C), and RNAPII (D) on MTAAT-gene target fragments in the TLBR-2 MTAAT^{KD} cell line. The values are representative of three independent experiments. (E) Box plots show the expression level of BNIP3 and BNIP3L in the cohort of formalin-fixed paraffin-embedded samples of anaplastic large cell lymphoma. One-tailed *t* test, **P*≤0.01. DOX: doxycycline; CTR: control.

eral mitochondrial proteins (cytochrome c oxidase subunit IV, superoxide dismutase, cytochrome, and prohibitin 1), assessed by western blot, confirmed these findings (Figure 5C). Since oxidative function is strictly linked to mitochondrial network dynamics, we evaluated the mitochondrial morphology of Mitotracker-stained cells using immunofluorescence. In a basal condition, ALK$^-$ ALCL cells showed the mitochondrial network predominantly distributed around the perinuclear region. Upon depletion of MTAAT, mitochondria displayed a more apical/basal localization which is indicative of a less active mitochondrial state[24] (Figure 5D). Concordantly, mitochondrial membrane potential, evaluated by TMRM staining, was reduced upon MTAAT^{KD}, suggesting mitochondrial dysfunction (Figure 5E). In line with these data, ALK$^-$ ALCL patients with high expression of MTAAT showed a high intensity and diffuse staining for superoxide dismutase compared to those expressing low levels of MTAAT (*Online Supplementary Figure S5A*).

Growing evidence points to a strong relationship between BNIP3, which acts as an adaptor for tethering mitochondria to nascent autophagosomes, and the activation of a selective form of macroautophagy known as mitophagy.[25] Having observed the overexpression of BNIP3 upon MTAAT^{KD}, we asked whether the observed changes in mitochondrial mass were due to the activation of mitophagy. First, we assessed whether canonical mitophagy markers can be detected upon MTAAT silencing. Notably, MTAAT^{KD} induced a time-dependent decrease of LC3 and of the autophagy receptor SQSTM1/p62 in both cell lines, suggestive of increased autophagy flux. Supporting this, treatment with chloroquine, an autophagy inhibitor that blocks the fusion of autophagosomes with lysosomes, blocked the MTAAT-dependent increase of autophagic flux (*Online Supplementary Figure S5B*). To strengthen these results, we analyzed the co-localization of specific mitophagy adaptors with autophagosomes. We co-transfected TLBR-2 cells with plasmids encoding LC3-GFP and BNIP3-Flag and analyzed their behavior upon MTAAT^{KD}. In control cells, both markers showed diffuse and homogeneous staining across the cytoplasm (Figure 6A). By contrast, upon MTAAT^{KD}, both LC3 and BNIP3

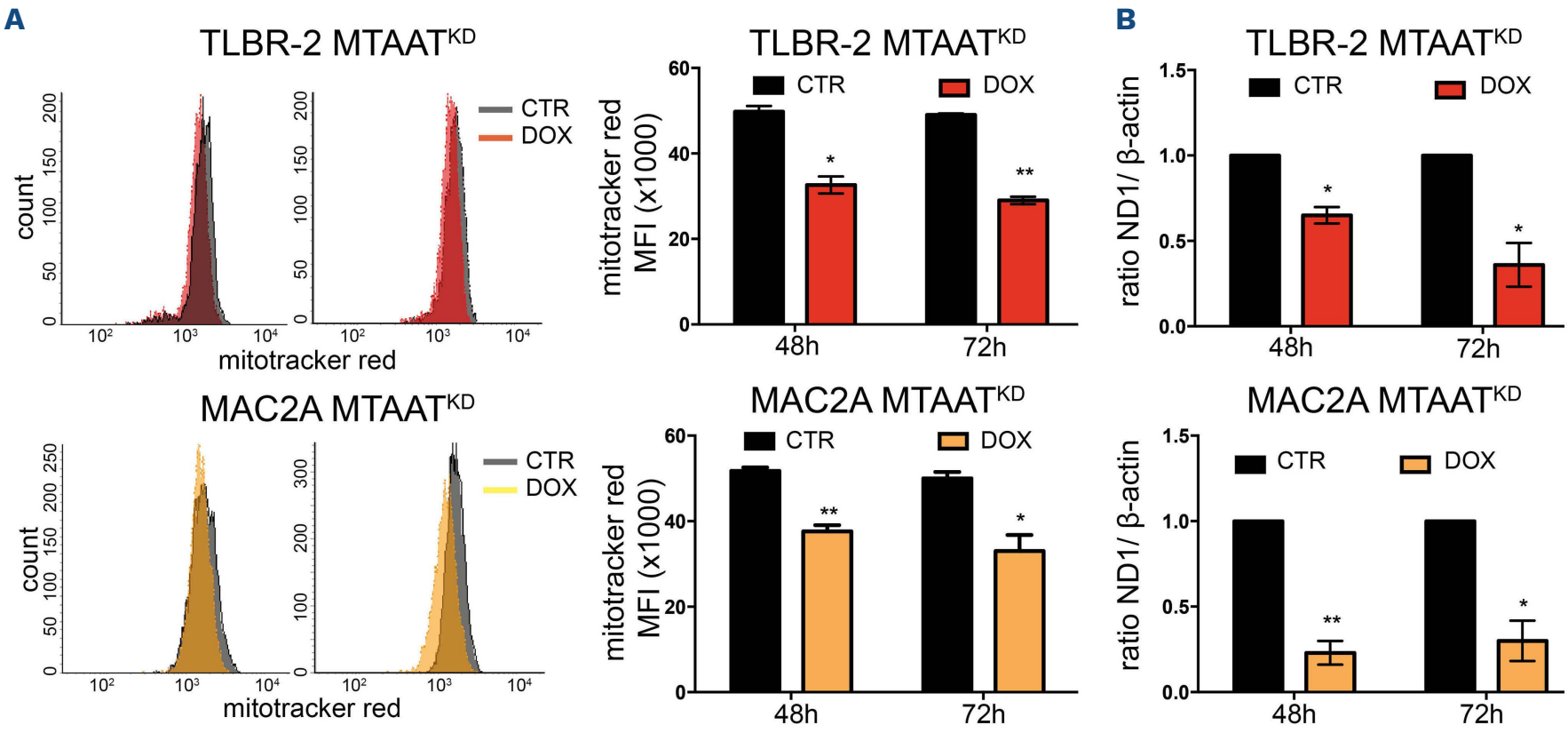

Figure 5. MTAAT inactivation impairs mitochondrial homeostasis. (A) Histograms of mean fluorescence intensity (MFI) assessed by flow cytometry analysis show a left shift of Mitotracker red fluorescence in MTAAT knockdown (MTAAT^{KD}) cell lines (red and yellow) compared to control (CTR, grey) at 48 and 72 h after doxycycline (DOX) treatment. Bar graphs show the MFI of cells stained with Mitotracker red and analyzed by FACS. Each datum represents the mean ± standard error of mean (SEM) (N=3). Two-tailed *t* test. **P*<0.05; ***P*<0.01 relative to the CTR. (B) Copy number analysis of the mitochondrial gene ND1 normalized on nuclear gene β-actin (48 and 72 h after DOX treatment). Each datum represents the mean ± SEM (N=3). Two-tailed *t* test, **P*<0.05; ***P*<0.01 relative to CTR. (C) Western blots show the expression of a set of mitochondrial proteins after MTAAT KD in TLBR-2 and MAC2A cells (72 h). (D) Immunofluorescence shows the localization of mitochondria in MTAAT^{KD} cells. Cells were stained with Mitotracker-red dye and DAPI. The white scale bar represents 10 μm. The adjacent bar graphs indicate the percentage of Mitotracker-red stained cells with apical/basal mitochondria (N=500 cells). Each datum represents the mean ± SEM (N=3). Two-tailed *t* test, **P*<0.05; ***P*<0.01 relative to CTR. (E) Histograms of FACS analysis show a right shift of tetramethylrhodamine methyl ester perchlorate (TMRM) fluorescence in MTAAT^{KD} cell lines (red and yellow) compared to the CTR (gray). Bar graphs show the MFI of cells stained with TMRM and analyzed by FACS. Each datum represents the mean ± SEM (N=3). Two-tailed *t* test, **P*<0.05; ***P*<0.01 relative to CTR. PHB1: prohibitin 1; SOD1: superoxide dismutase; COX IV: cytochrome c oxidase subunit IV; CytC: cytochrome C; α-TUB: α-tubulin.

accumulated into bright cytoplasmic puncta suggestive of LC3 lipidation and BNIP3 recruitment. Importantly, LC3 and BNIP3 puncta co-localize upon MTAAT^{KD} (Figure 6A), indicating active mitophagy.

We hypothesized that tumor cells specifically block mitophagy to increase mitochondrial mass and sustain proliferation. We, therefore, asked whether MTAAT^{KD} impacts ALK^{-} ALCL cell viability. Notably, growth curve analysis and viability assays showed that depleting MTAAT significantly reduced cellular proliferation in both TLBR-2 and MAC2A cell lines (Figure 6B). No changes were recorded in cell cycle profiles and apoptosis was not induced upon MTAAT^{KD}, consistent with energy deprivation, rather than cell death (*Online Supplementary Figure S5C, D*).

Collectively, our data support a model in which the lncRNA MTAAT exerts its function by stimulating an increase in mitochondrial mass – and energy output – which is used by ALK^{-} ALCL cells to sustain cell proliferation (Figure 6C).

Discussion

The implementation of digital gene expression profiling paved the way for application of a transcriptomic approach

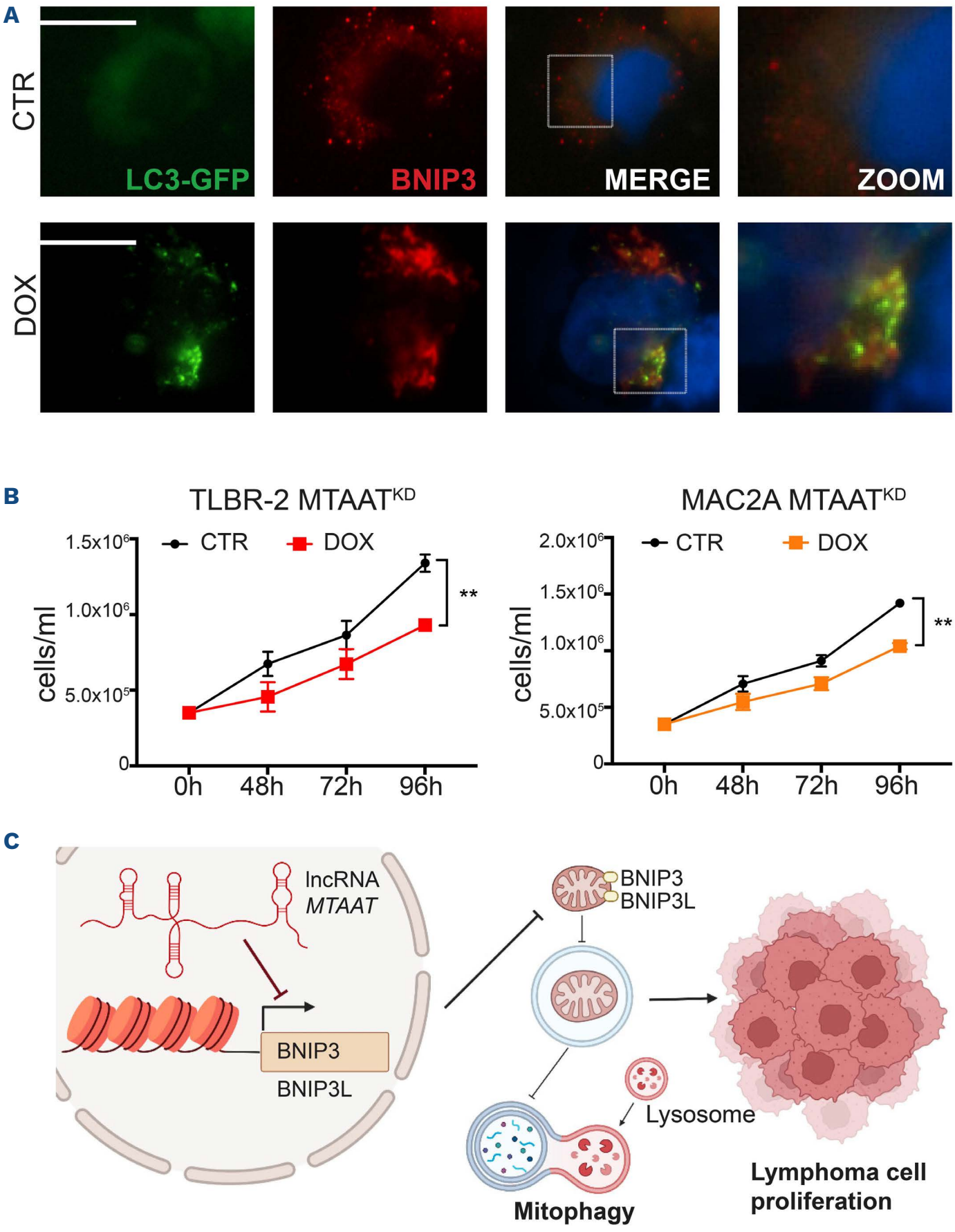

Figure 6. MTAAT knockdown promotes mitophagy and reduces cellular proliferation. (A) Immunofluorescence images of TLBR-2 MTAAT^{KD} cells after 48 h of doxycycline induction. Cells were stained with DAPI and FLAG antibodies for BNIP3 detection. The white scale bar represents 10 μm. (B) Growth curves show the proliferation of cells after MTAAT depletion. Each datum represents the mean ± standard error of mean (N=3). Two-tailed *t* test. ***P*<0.01 relative to the control. (C) Graphical model of MTAAT function in lymphoma. Figure created with BioRender.com. DOX: doxycycline; CTR: control; KD: knockdown.

to the classification of TCL, increasing the precision of diagnosis over conventional methods.[26] Progress toward understanding the transcriptional complexity of tumors revealed how coding genes are not the only drivers of cancer progression, with non-coding transcripts, such as lncRNA, regulating essential transcriptional cascades during tumorigenesis.[9,27,28] However, how lncRNA drive cellular and clinical phenotypes of aggressive TCL subtypes remains unknown.

In this study, we identified a set of lncRNA that act as molecular classifiers to distinguish ALK$^+$ and ALK$^-$ ALCL. We also report the role of one of these lncRNA, which we renamed MTAAT, in regulating mitochondrial turnover and progression of aggressive ALK$^-$ ALCL.

We identified MTAAT as significantly associated with the ALK$^-$ ALCL phenotype in two independent cohorts of ALCL patients: first from a cohort of FFPE diagnostic biopsies analyzed by digital expression profiling with the Nanostring nCounter platform and subsequently in a cohort of frozen tissues by RT-qPCR. We also demonstrated the high accuracy of MTAAT in predicting ALK$^-$ subtypes in ALCL classification. Although the use of lncRNA as biomarkers is still in its infancy, our results strongly suggest that digital lncRNA profiling could be integrated into diagnostic panels to improve the accuracy and precision of ALCL stratification.

We selected the lncRNA MTAAT for functional studies based on its association with ALK$^-$ ALCL. Analysis of the regulatory elements of MTAAT showed its intrinsic ability to regulate transcription. Transcriptional regulation by lncRNA appears to be a mechanism widely used by hematologic malignancies to control the transcription of selective pathways tuning aberrant proliferation and survival of B and T cells.[29-32]

By performing RNA sequencing on MTAAT^{KD} cell lines, we highlighted how the transcriptional program supported by MTAAT converges on the regulation of mitochondrial pathways. Mechanistic investigations showed that the loss of MTAAT is linked to a unique phenotype characterized by increased mitochondrial turnover through positive mitophagy stimulation, accompanied by a reduction in cell proliferation. Remarkably, lymphomas are characterized as oxidative tumors, indicating a requirement of mitochondrial function for tumor progression.[33,34] Mitochondria work as metabolic hubs to support cell growth and proliferation, and act as sensors of intracellular stresses that could threaten survival.[35,36] Although the role of mitophagy in lymphoid malignancies is still debated, some evidence indicates that the constitutive repression of autophagy/mitophagy contributes to lymphomagenesis.[37-41] The increase in the mitochondrial pool in tumor cells is also emerging as a key factor in the success of immunotherapeutic treatments,[42–44] such as chimeric antigen receptor-expressing T cells.[45] These chimeric antigen receptor-expressing cells represent an incredibly promising strategy for the treatment of several malignancies and for this reason, further investigations aimed at elucidating the role of MTAAT are warranted.

Among the downstream targets of MTAAT, we identified BNIP3 whose expression is upregulated upon MTAAT^{KD} via chromatin reorganization. BNIP3 was originally reported to function as a BH3-only protein which induced programmed cell death.[46,47] More recently, it has been shown to function as a stress-induced mitophagy receptor that interacts directly with LC3 to promote the turnover of otherwise healthy mitochondria.[48,49] Although various human solid cancers overexpress BNIP3 as they become hypoxic,[50] inactivation of BNIP3 via promoter hypermethylation is a common feature of aggressive and advanced-stage cancers such as triple-negative breast cancer, hematologic malignancies and advanced-stage pancreatic cancer.[51-54] In these tumors, epigenetic silencing of BNIP3 correlates with high cancer cell proliferation, poor prognostic features, and chemoresistance.[55,56] In accordance with this observation, we found a significant reduction of BNIP3 expression in a cohort of ALK$^-$ ALCL patients. This finding suggests a tumor-suppressive function of BNIP3 also in the context of ALCL. We speculate that the loss of BNIP3 associated with reduced mitophagy may create a more aggressive tumor phenotype and contribute, at least in part, to the chemoresistance observed in this malignancy. This evidence paves the way for the implementation of targeted therapeutic strategies able to re-express BNIP3 in this lymphoid malignancy.

In conclusion, we have characterized the novel lncRNA MTAAT as a new potential biomarker in the stratification of ALCL patients. Functionally, MTAAT acts as a transcriptional brake on mitophagy, promoting the accumulation of mitochondria and supporting lymphoma progression. These findings corroborate our previous data showing a key role of lncRNA in the control of different transcriptional programs in ALK$^-$ ALCL.

Disclosures

No conflicts of interest to disclose.

Contributions

VM and AT performed experiments and analyzed data, BD performed gene expression and Nanostring analyses, VM, FT, ES, and EV performed RNA-sequencing, ChIP-sequencing, and bioinformatics analyses. FR performed FACS analyses and cell sorting experiments, MZ, SA, GI, FS, CF, MP, AR, GM, SL, APDS, and AB provided tissue samples and lymphoma diagnosis. MT and AN provided important experimental and analytic support. AC interpreted the results and helped to discuss the results. VF designed the project, interpreted the results, and wrote the manuscript. All the authors read and approved the final version of the manuscript.

Acknowledgments

The authors are grateful to Marina Grassi, Ione Tamagnini, Gloria Venturini, and Riccardo Fuoco for technical help and to all the members of the laboratory for helpful discussion.

Funding

VM and AT were supported by Fondazione AIRC per la Ricerca sul Cancro (AIRC). FR was supported by Fondazione Umberto Veronesi. VM and AR were supported by Fondazione GRADE Onlus. This study was funded by the Italian Ministry of Health through Ricerca Finalizzata (N. GR-2016-02364298, to VF), Bando per la Valorizzazione della Ricerca Istituzionale 2021- fondi 5 per Mille 2020 (to VF) and Fondazione AIACE (to VF). The study was also partially supported by the Italian Ministry of Health-Ricerca Corrente Annual Program 2024.

Data-sharing statement

All data generated and/or analyzed in this study are included in this article and its Online Supplementary Appendix. The MTAAT sequence has been deposited in the GenBank database with accession number OM642832. Gene expression profile data are available at the Gene Expression Omnibus (GEO) repository (accession number: GSE217426). RNA-sequencing raw data in fastq.gz format are available in the ArrayExpress repository, dataset E-MTAB-12462 (https://www.ebi.ac.uk/arrayexpress/experiments/E-MTAB-12462).

References

1. Swerdlow SH, Campo E, Pileri SA, et al. The 2016 revision of the World Health Organization classification of lymphoid neoplasms. Blood. 2016;127(20):2375-2390.
2. Ferreri AJM, Govi S, Pileri SA, Savage KJ. Anaplastic large cell lymphoma, ALK-negative. Crit Rev Oncol Hematol. 2013;85(2):206-215.
3. Parrilla Castellar ER, Jaffe ES, Said JW, et al. ALK-negative anaplastic large cell lymphoma is a genetically heterogeneous disease with widely disparate clinical outcomes. Blood. 2014;124(9):1473-1480.
4. Savage KJ, Harris NL, Vose JM, et al. ALK– anaplastic large-cell lymphoma is clinically and immunophenotypically different from both ALK+ ALCL and peripheral T-cell lymphoma, not otherwise specified: report from the International Peripheral T-Cell Lymphoma Project. Blood. 2008;111(12):5496-5504.
5. Fiore D, Cappelli LV, Broccoli A, Zinzani PL, Chan WC, Inghirami G. Peripheral T cell lymphomas: from the bench to the clinic. Nat Rev Cancer. 2020;20(6):323-342.
6. Rheinbay E, Nielsen MM, Abascal F, et al for the PCAWG Drivers and Functional Interpretation Working Group, PCAWG Structural Variation Working Group, and PCAWG Consortium. Analyses of non-coding somatic drivers in 2,658 cancer whole genomes. Nature. 2020;578(7793):102-111.
7. van Galen P. Decoding the noncoding cancer genome. Cancer Discov. 2020;10(5):646-647.
8. Kapranov P, Cheng J, Dike S, et al. RNA maps reveal new RNA classes and a possible function for pervasive transcription. Science. 2007;316(5830):1484-1488.
9. Statello L, Guo C-J, Chen L-L, Huarte M. Gene regulation by long non-coding RNAs and its biological functions. Nat Rev Mol Cell Biol. 2021;22(2):96-118.
10. Marchese FP, Raimondi I, Huarte M. The multidimensional mechanisms of long noncoding RNA function. Genome Biol. 2017;18(1):206.
11. Goff LA, Rinn JL. Linking RNA biology to lncRNAs. Genome Res 2015;25(10):1456-1465.
12. Ransohoff JD, Wei Y, Khavari PA. The functions and unique features of long intergenic non-coding RNA. Nat Rev Mol Cell Biol. 2018;19(3):143-157.
13. Huarte M. The emerging role of lncRNAs in cancer. Nat Med. 2015;21(11):1253-1261.
14. Anastasiadou E, Jacob LS, Slack FJ. Non-coding RNA networks in cancer. Nat Rev Cancer. 2018;18(1):5-18.
15. Iannello A, Ciarrocchi A, Fragliasso V, Vaisitti T. Lift the curtain on long non-coding RNAs in hematological malignancies: pathogenic elements and potential targets. Cancer Lett. 2022;536:215645.
16. Fragliasso V, Verma A, Manzotti G, et al. The novel lncRNA BlackMamba controls the neoplastic phenotype of ALK– anaplastic large cell lymphoma by regulating the DNA helicase HELLS. Leukemia. 2020;34(11):2964-2980.
17. Tameni A, Sauta E, Mularoni V, et al. The DNA-helicase HELLS drives ALK– ALCL proliferation by the transcriptional control of a cytokinesis-related program. Cell Death Dis. 2021;12(1):130.
18. Fragliasso V, Chiodo Y, Ferrari-Amorotti G, et al. Phosphorylation of serine 21 modulates the proliferation inhibitory more than the differentiation inducing effects of C/EBPα in K562 cells. J Cell Biochem. 2012;113(5):1704-1713.
19. Agnelli L, Mereu E, Pellegrino E, et al. Identification of a 3-gene model as a powerful diagnostic tool for the recognition of ALK-negative anaplastic large-cell lymphoma. Blood. 2012;120(6):1274-1281.
20. Grant CE, Bailey TL, Noble WS. FIMO: scanning for occurrences of a given motif. Bioinformatics. 2011;27(7):1017-1018.
21. Sandoval H, Thiagarajan P, Dasgupta SK, et al. Essential role for Nix in autophagic maturation of erythroid cells. Nature. 2008;454(7201):232-235.
22. O'Sullivan TE, Johnson LR, Kang HH, Sun JC. BNIP3- and BNIP3L-mediated mitophagy promotes the generation of natural killer cell memory. Immunity. 2015;43(2):331-342.
23. Bellucci M, Agostini F, Masin M, Tartaglia GG. Predicting protein associations with long noncoding RNAs. Nat Methods. 2011;8(6):444-445.
24. Facucho-Oliveira JM, St. John JC. The relationship between pluripotency and mitochondrial DNA proliferation during early embryo development and embryonic stem cell differentiation. Stem Cell Rev Rep. 2009;5(2):140-158.
25. Youle RJ, Narendra DP. Mechanisms of mitophagy. Nat Rev Mol Cell Biol. 2011;12(1):9-14.
26. Amador C, Bouska A, Wright G, et al. Gene expression signatures for the accurate diagnosis of peripheral T-cell lymphoma entities in the routine clinical practice. J Clin Oncol. 2022;40(36):4261-4275.
27. Palazzo AF, Koonin EV. Functional long non-coding RNAs evolve

from junk transcripts. Cell. 2020;183(5):1151-1161.
28. Schmitt AM, Chang HY. Long noncoding RNAs in cancer pathways. Cancer Cell. 2016;29(4):452-463.
29. Doose G, Haake A, Bernhart SH, et al. MINCR is a MYC-induced lncRNA able to modulate MYC's transcriptional network in Burkitt lymphoma cells. Proc Natl Acad Sci U S A. 2015;112(38):E5261-5270.
30. Zhao P, Ji M-M, Fang Y, et al. A novel lncRNA TCLlnc1 promotes peripheral T cell lymphoma progression through acting as a modular scaffold of HNRNPD and YBX1 complexes. Cell Death Dis. 2021;12(4):321.
31. Zhao C-C, Jiao Y, Zhang Y-Y, et al. Lnc SMAD5-AS1 as ceRNA inhibit proliferation of diffuse large B cell lymphoma via Wnt/β-catenin pathway by sponging miR-135b-5p to elevate expression of APC. Cell Death Dis. 2019;10(4):252.
32. Cui Y, Xu H, Yang Y, et al. The regulation of miR-320a/XBP1 axis through LINC00963 for endoplasmic reticulum stress and autophagy in diffuse large B-cell lymphoma. Cancer Cell Int. 2021;21(1):305.
33. Li M, Teater MR, Hong JY, et al. Translational activation of ATF4 through mitochondrial anaplerotic metabolic pathways is required for DLBCL growth and survival. Blood Cancer Discov. 2022;3(1):50-65.
34. Bhalla K, Jaber S, Nahid MN, et al. Role of hypoxia in diffuse large B-cell lymphoma: metabolic repression and selective translation of HK2 facilitates development of DLBCL. Sci Rep. 2018;8(1):744.
35. Giacomello M, Pyakurel A, Glytsou C, Scorrano L. The cell biology of mitochondrial membrane dynamics. Nat Rev Mol Cell Biol. 2020;21(4):204-224.
36. Eisner V, Picard M, Hajnóczky G. Mitochondrial dynamics in adaptive and maladaptive cellular stress responses. Nat Cell Biol. 2018;20(7):755-765.
37. Bertolo C, Roa S, Sagardoy A, et al. LITAF , a BCL6 target gene, regulates autophagy in mature B-cell lymphomas. Br J Haematol. 2013;162(5):621-630.
38. Wang Z, Xu F, Yuan N, et al. Rapamycin inhibits pre-B acute lymphoblastic leukemia cells by downregulating DNA and RNA polymerases. Leuk Res. 2014;38(8):940-947.
39. Cheng C, Wang T, Song Z, et al. Induction of autophagy and autophagy-dependent apoptosis in diffuse large B-cell lymphoma by a new antimalarial artemisinin derivative, SM1044. Cancer Med. 2018;7(2):380-396.
40. Nahimana A, Attinger A, Aubry D, et al. The NAD biosynthesis inhibitor APO866 has potent antitumor activity against hematologic malignancies. Blood. 2009;113(14):3276-3286.
41. Torossian A, Broin N, Frentzel J, et al. Blockade of crizotinib-induced BCL2 elevation in ALK-positive anaplastic large cell lymphoma triggers autophagy associated with cell death. Haematologica. 2019;104(7):1428-1439.
42. Sainero-Alcolado L, Liaño-Pons J, Ruiz-Pérez MV, Arsenian-Henriksson M. Targeting mitochondrial metabolism for precision medicine in cancer. Cell Death Differ. 2022;29(7):1304-1317.
43. Missiroli S, Perrone M, Genovese I, Pinton P, Giorgi C. Cancer metabolism and mitochondria: finding novel mechanisms to fight tumours. eBioMedicine 2020;59:102943.
44. Porporato PE, Filigheddu N, Pedro JMB-S, Kroemer G, Galluzzi L. Mitochondrial metabolism and cancer. Cell Res. 2018;28(3):265-280.
45. Zhang L, Zhang W, Li Z, et al. Mitochondria dysfunction in CD8+ T cells as an important contributing factor for cancer development and a potential target for cancer treatment: a review. J Exp Clin Cancer Res. 2022;41(1):227.
46. Chen G, Ray R, Dubik D, et al. The E1B 19K/Bcl-2–binding protein Nip3 is a dimeric mitochondrial protein that activates apoptosis. J Exp Med. 1997;186(12):1975-1983.
47. Ray R, Chen G, Vande Velde C, et al. BNIP3 heterodimerizes with Bcl-2/Bcl-XL and induces cell death independent of a Bcl-2 homology 3 (BH3) domain at both mitochondrial and nonmitochondrial sites. J Biol Chem. 2000;275(2):1439-1448.
48. Hanna RA, Quinsay MN, Orogo AM, Giang K, Rikka S, Gustafsson ÅB. Microtubule-associated protein 1 light chain 3 (LC3) interacts with Bnip3 protein to selectively remove endoplasmic reticulum and mitochondria via autophagy. J Biol Chem. 2012;287(23):19094-19104.
49. Glick D, Zhang W, Beaton M, et al. BNip3 regulates mitochondrial function and lipid metabolism in the liver. Mol Cell Biol. 2012;32(13):2570-2584.
50. Sowter HM, Ferguson M, Pym C, et al. Expression of the cell death genes BNip3 and NIX in ductal carcinoma in situ of the breast; correlation of BNip3 levels with necrosis and grade. J Pathol. 2003;201(4):573-580.
51. Chourasia AH, Tracy K, Frankenberger C, et al. Mitophagy defects arising from BNip3 loss promote mammary tumor progression to metastasis. EMBO Rep. 2015;16(9):1145-1163.
52. Koop EA, van Laar T, van Wichen DF, de Weger RA, van der Wall E, van Diest PJ. Expression of BNIP3 in invasive breast cancer: correlations with the hypoxic response and clinicopathological features. BMC Cancer. 2009;9(1):175.
53. Murai M, Toyota M, Satoh A, et al. Aberrant DNA methylation associated with silencing BNIP3 gene expression in haematopoietic tumours. Br J Cancer. 2005;92(6):1165-1172.
54. Okami J, Simeone DM, Logsdon CD. Silencing of the hypoxia-inducible cell death protein BNIP3 in pancreatic cancer. Cancer Res. 2004;64(15):5338-5346.
55. Akada M, Crnogorac-Jurcevic T, Lattimore S, et al. Intrinsic chemoresistance to gemcitabine is associated with decreased expression of BNIP3 in pancreatic cancer. Clin Cancer Res. 2005;11(8):3094-3101.
56. Erkan M, Kleeff J, Esposito I, et al. Loss of BNIP3 expression is a late event in pancreatic cancer contributing to chemoresistance and worsened prognosis. Oncogene. 2005;24(27):4421-4432.